8-1-2009

Determining Azimuthal Variations in Frontal Froude Number from SAR Imagery

Jiayi Pan
Portland State University

David A. Jay
Portland State University

Hui Lin

Citation Details

Pan, J., D. A. Jay, and H. Lin (2009), Determining azimuthal variations in frontal Froude number from SAR imagery, Geophys. Res. Lett., 36, L15601.

Determining azimuthal variations in frontal Froude number from SAR imagery

Jiayi Pan,[1,2] David A. Jay,[2] and Hui Lin[1]

Received 6 May 2009; revised 8 June 2009; accepted 30 June 2009; published 1 August 2009.

[1] River plume fronts are the locus of strong mixing between plume and ambient coastal waters, contribute to coastal productivity, and exert a major impact on coastal ecosystems. The frontal Froude number *Fr* is an important parameter characterizing the frontal status with respect to both propagation and vertical mixing. In this study, we examine azimuthal variations in *Fr* using a new remote sensing method. We derive *Fr* from SAR image data on the basis of the SAR imaging theory and the mechanism of internal wave fission at front. This method is applied to a SAR image showing a front off the Columbia River (CR) mouth taken on 31 May 2003 at 14:33:19 UTC under weak wind conditions. *Fr* increases from south to north along the front. This variation is consistent with potential vorticity conservation and the influence of tidal currents on the plume. This calculation confirms arguments based on vessel observations by Jay et al. (2009). **Citation:** Pan, J., D. A. Jay, and H. Lin (2009), Determining azimuthal variations in frontal Froude number from SAR imagery, *Geophys. Res. Lett.*, *36*, L15601, doi:10.1029/2009GL039068.

1. Introduction

[2] Much of interaction between river plumes and the coastal ocean occurs at the front of each successive ebb tidal pulse [*Pritchard and Huntley*, 2002; *Luketina and Imberger*, 1989]. Tidal plume fronts exhibit vigorous mixing and disturb the seabed, dissipating the plume energy and mixing upwelled nutrients and iron (Fe) from re-suspended river sediments into the surface layer [*Orton and Jay*, 2005]. Despite high plume stratification, more upwelled nutrients (N and P) and Fe may reach the surface in the plume area than outside of it. The Columbia River (CR) plume, for example, is highly productive and contributes to regional primary production, especially the plume front [*Jay et al.*, 2009; *Hickey et al.*, 2009].

[3] *Simpson and Britter* [1980] suggested that as the frontal Froude number (*Fr*, the ratio of frontal speed to the internal wave speed) increases, frontal entrainment goes up. *Pritchard and Huntley* [2006] reported that mixing was high in the supercritical ($Fr > 1$) frontal region of the buoyant outflow from the estuary of the River Teign in the UK. *Orton and Jay* [2005] found locally strong mixing at the CR plume front with an eddy diffusivity of $O(0.2\ m^2\ s^{-1})$ 50 m behind the front. Non-linear internal waves (NLIWs) can be generated at and propagate offshore from the plume front as it transitions from a supercritical to subcritical state [*Nash and Moum*, 2005]. *Jay et al.* [2009] reported that there are obvious differences in internal wave generation at upstream fronts between upwelling and downwelling conditions. *Horner-Devine et al.* [2009] defined plume anatomy using the supercritical front around the tidal plume (the most recent outflow) to distinguish the tidal plume from the near-field that has been at sea for several days. Once the tidal plume front becomes subcritical, the tidal plume merges into the near-field.

[4] These observations suggest that the frontal Froude number is a very important parameter characterizing river plume frontal behavior. In this study, we introduce a method to estimate plume the frontal *Fr* using satellite Synthetic Aperture Radar (SAR) images. A SAR collects high resolution (~10 m) images of ocean surface, and captures spatial features of internal waves and fronts. The study uses SAR imagery in CR plume region in a new way to determine the spatial variation of *Fr* along the tidal plume front.

2. Methodology

[5] SAR image intensity is related to the spectral density of ocean surface waves. Satellite SARs work at the cm-wavelengths and are tuned to be in Bragg resonance with surface gravity-capillary waves that are the dominant scatterers, and the SAR radar backscatter cross section per unit area is determined by the spectral density of gravity-capillary waves [*Plant*, 1990]. A spectral density function for gravity-capillary waves was derived by *Yuan* [1997] and consists of three components representing the wind-input, surface tension, and wave-current interaction terms, respectively. At the scale of a river plume front, it is reasonable to take the wind-input and surface tension terms as constants that affect only the background wave spectral density. Therefore, spatial variations in the SAR image intensity associated with the river front are determined only by the wave-current interaction term. This term is proportional to the convergence of the surface velocity. Thus, taking into account the SAR beam looking angle (φ) relative to the front normal direction (Figure 1), the radar cross section σ_0 associated with the front is proportional to the velocity convergence [*Zheng et al.*, 2001; *Pan et al.*, 2007]

$$\sigma_0 \propto \cos\phi\left[-\frac{\partial\left(u|_{z=0}\right)}{\partial x}\right]. \quad (1)$$

Strong convergence occurs at the plume front. Thus, the front is characterized by a bright line in a SAR image.

[1]Institute of Space and Earth Information Science, Chinese University of Hong Kong, Shatin, Hong Kong.
[2]Department of Civil and Environmental Engineering, Portland State University, Portland, Oregon, USA.

0094-8276/09/2009GL039068

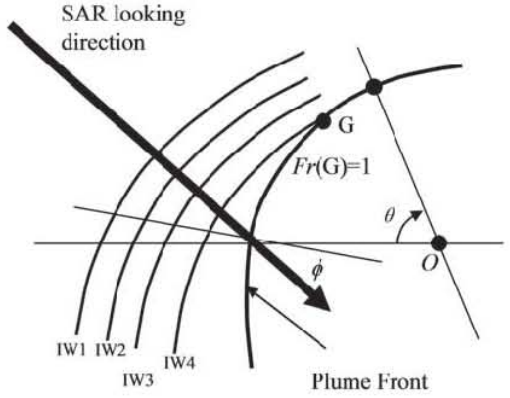

Figure 1. Schematic map of a plume front and frontal internal waves.

The integral of the radar backscatter cross section across the front line is

$$\int_{S1}^{S2} \sigma_0 dx = C \cos\phi \left(U_f - U_a\right), \tag{2}$$

where x is in cross-front direction; $S1$ and $S2$ represent the positions on both sides of the front (Figure 2); U_f is velocity in the frontal area, namely the speed of the plume behind the front; U_a is ambient velocity, representing ambient speed of the old plume water outside the front; and C is a constant. We consider here a coordinate system perpendicular to the front, and U_f and U_a are the local velocity components perpendicular to the front, just within and outside the front, respectively. The frontal Froude number is the ratio of the frontal phase speed (U_f') to the internal wave speed (c). In the presence of an ambient (normal) current (U_a), Fr is written as [*Pritchard and Huntley*, 2002]

$$Fr = \left(U_f' - U_a\right)/c, \tag{3}$$

A coefficient, β is defined by *Pritchard and Huntley* [2002]

$$\beta = \left(U_f - U_f'\right)/\left(U_f' - U_a\right) = \left(U_f - U_a\right)/\left(U_f' - U_a\right) - 1. \tag{4}$$

Therefore, the Froude number is derived as

$$Fr = \frac{1}{\beta + 1}\frac{\left(U_f - U_a\right)}{c}, \tag{5}$$

where $\frac{1}{\beta+1}$ can be regarded as nearly constant along the plume front. There is often a fission point at the river plume front, where an internal wave is being generated and the frontal Froude number is critical: $Fr = 1$ (cf. point G in Figure 1) [*Nash and Moum*, 2005; *Jay et al.*, 2009]. At point G, the relative frontal radial speed equals the internal wave phase speed in the ambient water; thus,

$$Fr_G = \left(U_f' - U_a\right)/c = 1. \tag{6}$$

Therefore, we have

$$\frac{1}{\beta + 1}\left(U_{fG} - U_{aG}\right) = c, \tag{7}$$

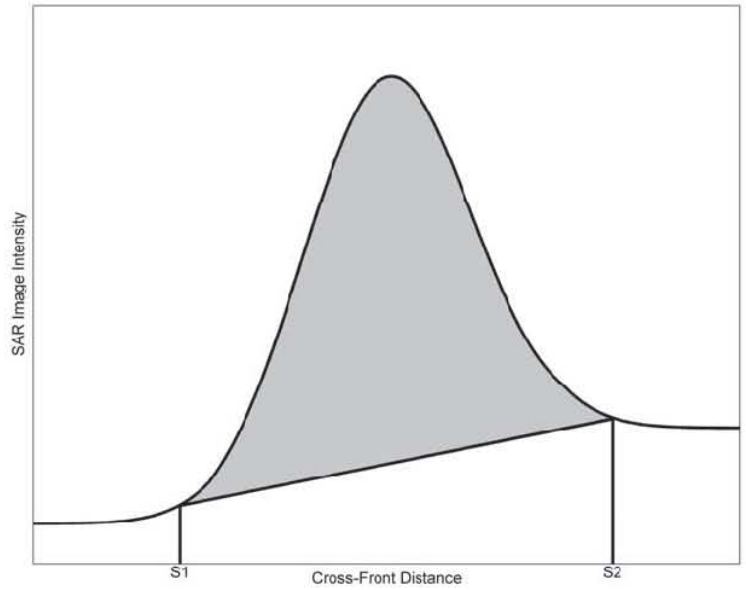

Figure 2. Schematic map of SAR image intensity profile across the front.

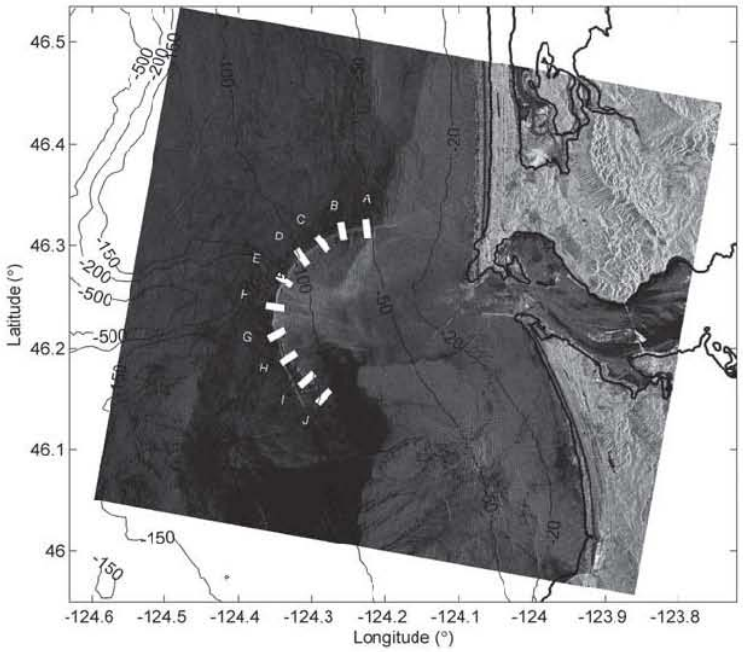

Figure 3. A SAR image taken on 31 May 2003 at 14:33:19 UTC showing the CR plume front and an internal wave. There are ten rectangle boxes across the front line marked as A, B, C, D, E, F, G, H, I, and J. The bathymetry contours are in meters.

and

$$\int_{S1_G}^{S2_G} \sigma_{0G} dx = C \cos\phi_G (U_{fG} - U_{aG}). \tag{8}$$

Combination of (7) and (8) yields

$$c = \frac{1}{C(\beta+1)\cos\phi_G} \int_{S1_G}^{S2_G} \sigma_{0G} dx. \tag{9}$$

From (2) and (9), we derive the frontal Froude number

$$Fr(\theta) = \frac{U_f' - U_a}{c} = \frac{(U_f - U_a)}{(\beta+1)c} = \frac{\cos\phi_G \int_{S1}^{S2} \sigma_0 dx}{\cos\phi \int_{S1_G}^{S2_G} \sigma_{0G} dx}. \tag{10}$$

The frontal location is characterized by the azimuthal angle θ, shown in Figure 1, in which point O represents the center of the nearly radial plume front. Thus, knowledge of Fr at one point on the front suffices to determine it along the entire visible front. Note that the calculated Fr numbers are defined in the frame of reference perpendicular to the front, and not parallel to the local flow velocity.

3. SAR Image Analyses

[6] The SAR image used in this study was taken on 31 May 2003 at 14:33:19 UTC by RADARSAT-1 SAR, and processed at the Alaska Satellite Facility in Fairbanks, Alaska. This image (Figure 3) shows a CR plume front separating the plume water from the ambient coastal water; there was an internal wave traveling seaward from the front. Internal wave fission was occurring at point G, at the intersection of the frontal line and the internal wave crest line. Winds were weak southerlies with a direction and speed about 200° and 1 m s^{-1}, respectively. The image time was about 6.5 hrs after the higher high water at the estuary mouth, indicating that the front was associated with the most recent ebb.

[7] In order to calculate the Fr along the front, we select 10 rectangle areas across the front and they are marked as A, B, C, . . ., J in Figure 3. In each white rectangular box, we choose 10 sections across the front, and obtain 10 SAR image intensity profiles. To reduce the image noise, each group of 10 sectional profiles is averaged. The averaged SAR image intensity (SII) profiles (Figures 4a–4h) show that peaks in the image intensity sectional profiles are associated with the plume front. Figure 4h reveals strong dual peaks; the left one represents the internal wave and the right one is the front. The beginning and ending points for the integration in (10) are deduced from the SAR image and marked as S1 and S2 in Figures 4a–4h. To obtain the integral in (10), we need to subtract the SAR image background contributions from the image data. The method is described as follows. The integral of the image intensity (SII) over the distance from S1 to S2 is (Figure 2)

$$Q_1 = \int_{S1}^{S2} SII(x) dx. \tag{11}$$

[8] The background is given by

$$Q_2 = (S2 - S1)[SII(S1) + SII(S2)]/2. \tag{12}$$

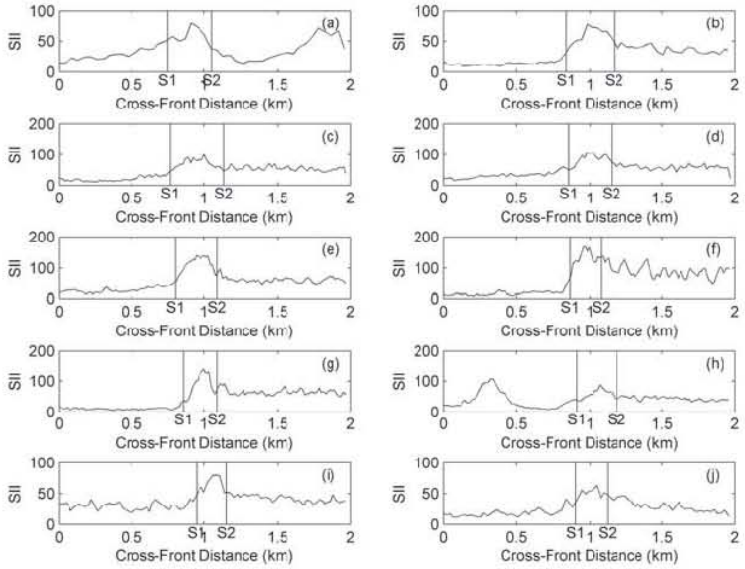

Figure 4. The averaged the SAR image intensity (SII) profiles across the frontal line for boxes (a) A, (b) B, (c) C, (d) D, (e) E, (f) F, (g) G, (h) H, (i) I, and (j) J, where S1 and S2 are the boundaries of the front deduced from the SAR image.

The integral of the SAR image intensity without the background contributions is

$$Q = Q_1 - Q_2, \tag{13}$$

Q is the area of the shaded region in Figure 2. For the data in Figure 4, Q is calculated from equations (11)–(13), and Fr for A–J is obtained from equation (10); results are listed in Table 1, along with $\cos\varphi$.

[9] The calculated Fr along the front is shown in Figure 5, in which x-axis represents the distance along the front line with the positive direction to the north and the origin at the internal wave fission point. Figure 5 suggests that the Froude number is increasing from south to north along the front line except at section C.

[10] To understand the observed along-frontal variations in Fr, some mesoscale context is needed. Winds at the time of this SAR image were downwelling favorable but weak, sufficient to stop coastal upwelling, but not strong enough to displace the larger CR plume to the north. The CR tidal plume is initially supercritical with respect to Fr on all stronger ebbs. *Jay et al.* [2009] observed that when the front is supercritical, it is sharp and narrow (only ~20–100 m wide on its upwind or northern side, cf. Figure 3) and marks a transition from supercritical to subcritical flow for up to 12 hours after high water. Supercritical plume fronts often generate NLIW trains as they slow and transition to a subcritical state. Moreover, NLIW formation almost always begins on the south side of the plume so that the front "unzips" from south to north, as shown in Figure 1. This implies that a frontal transition from supercritical to subcritical conditions first occurs on the south side tidal plume, regardless of whether this is the upwind or downwind side of the plume.

[11] *Jay et al.* [2009] suggested that there are two reasons for the observed frontal asymmetry, at least during the summer season. First, there is not a perfect reversal of alongshore currents between south and north – currents to the south are usually stronger than northward currents. This disproportionately sharpens convergence on the north side of the plume. Potential vorticity conservation provides a second mechanism. The equations for potential vorticity and mass conservation for a surface layer (assumed vertically uniform) are

$$d[(f+\xi)/H]/dt = 0, \tag{14}$$

and

$$\nabla_h \mathbf{U} = -\frac{1}{H} dH/dt, \tag{15}$$

where ξ is relative vorticity and H is the plume depth. The initial condition as the front emerges is that $\xi = 0$ ($\partial u/\partial y = 0$) in mid-outflow. For northward turning plume waters, the divergent tidal flow beneath the plume causes ξ to decrease, so $\xi < 0$. Given that changes in f are very small over the

Table 1. Calculated Froude Number

	A	B	C	D	E	F	G	H	I	J
θ	84.0	79.7	51.6	55.0	34.7	10.2	−28.5	−32.9	−42.2	−45.0
Fr	2.5	2.1	1.4	1.5	1.4	1.2	1.0	0.9	0.8	0.8
$\cos\varphi$	0.28	0.35	0.75	0.71	0.91	1.0	0.78	0.73	0.61	0.57

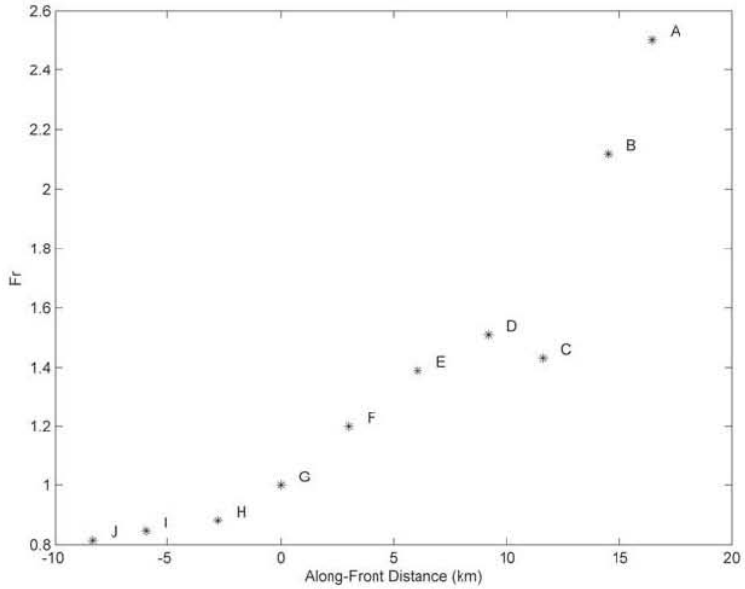

Figure 5. Froude number along the front. The x-axis is the distance along the front with the origin at the fission point (*G*) and the positive value to the north and the negative to the south.

scale of the tidal plume, H must [from (14)] decrease, thinning the northern plume front to maintain its rapid movement and keeping Fr high. (Changes in Fr near the front are controlled primarily by velocity changes [*Nash and Moum*, 2005].) In contrast, the divergent tidal flow beneath the plume causes ξ to increase for southward turning waters, producing a lower Fr. Thus, we expect an increase in Fr northward along the front. Plume expansion will eventually cause a transition to subcritical conditions ($Fr < 1$), and frontal energy is lost by a pulse of NLIW generation, but this will occur first on the south side of the plume. While there a turbulent frictional energy loss at the base of the plume – and this momentum exchange is required for the tidal vorticity transfer described above, the inviscid form of potential vorticity conservation (14) provides a simple, qualitatively correct description.

[12] The above suggests that the Columbia River plume front should frequently be seen as asymmetric in SAR images both in terms of Fr and mixing status. To the north, the front is sharp and mixing is strong, and to the south, it is diffuse with less mixing. This is consistent with Froude number calculation in this paper, which shows that the Froude number increases from south to north except location *C* (Figure 5). The anomaly at *C* could result from noise in the SAR image or from small-scale frontal phenomenon – the front is not perfectly two-dimensional.

4. Summary

[13] SAR images capture sea surface backscatter of radar signals, which is related to the surface spectral density of gravity-capillary waves and proportional to the velocity convergence. Based on this principle, we develop a new method to estimate the river plume frontal Froude number from SAR images and apply it to a SAR image showing a plume front and an internal wave in the CR plume region under the weak downwelling condition. Result shows that Fr increases from south to north along the front, a result that has been explained by vorticity conservation and interaction with alongshore currents. The SAR image-based method we advance here makes it much easier to determine azimuthal Fr variations (the front evolves so rapidly that no two passes of a single vessel across it can be considered synoptic) and is useful in testing models and theories of buoyant plumes.

[14] **Acknowledgments.** The study was primarily supported by the National Science Foundation (project OCE 0851527). It was also partially supported by the Direct Grant of the Chinese University of Hong Kong. The SAR image was provided by Comprehensive Large Array-data Stewardship System (CLASS) of NOAA. The authors are grateful to the anonymous reviewers for their valuable suggestions and comments.

References

Hickey, B., R. McCabe, S. Geier, E. Dever, and N. Kachel (2009), Three interacting freshwater plumes in the northern California Current System, *J. Geophys. Res.*, *114*, C00B03, doi:10.1029/2008JC004907.

Horner-Devine, A., D. A. Jay, P. M. Orton, and E. Spahn (2009), A conceptual model of the strongly tidal Columbia River plume, *J. Mar. Syst.*, in press.

Jay, D. A., J. Pan, P. M. Orton, and A. Horner-Devine (2009), Asymmetry of tidal plume fronts in an eastern boundary current regime, *J. Mar. Syst.*, in press.

Luketina, D. A., and J. Imberger (1989), Turbulence and entrainment in a buoyant surface plume, *J. Geophys. Res.*, *94*, 12,619–12,636, doi:10.1029/JC094iC09p12619.

Nash, J. D., and J. N. Moum (2005), River plumes as a source of large-amplitude internal waves in the coastal ocean, *Nature*, *437*, 400–403, doi:10.1038/nature03936.

Orton, P. M., and D. A. Jay (2005), Observations at the tidal plume front of a high-volume river outflow, *Geophys. Res. Lett.*, *32*, L11605, doi:10.1029/2005GL022372.

Pan, J., D. A. Jay, and P. M. Orton (2007), Analyses of internal solitary waves generated at the Columbia River plume front using SAR imagery, *J. Geophys. Res.*, *112*, C07014, doi:10.1029/2006JC003688.

Plant, W. J. (1990), Bragg scattering of electromagnetic waves from the air/sea interface, in *Surface Waves and Fluxes*, vol. 2, *Remote Sensing*, edited by G. L. Geernaet and W. J. Plant, pp. 41–168, Kluwer Acad., Norwell, Mass.

Pritchard, M., and D. A. Huntley (2002), Instability and mixing in a small estuarine plume front, *Estuarine Coastal Shelf Sci.*, *55*, 275–285, doi:10.1006/ecss.2001.0902.

Pritchard, M., and D. A. Huntley (2006), A simplified energy and mixing budget for a small river plume discharge, *J. Geophys. Res.*, *111*, C03019, doi:10.1029/2005JC002984.

Simpson, J. E., and R. E. Britter (1980), A laboratory model of an atmospheric meso-front, *Q. J. R. Meteorol. Soc.*, *106*, 485–500, doi:10.1002/qj.49710644907.

Yuan, Y. (1997), Representation of high frequency spectra of ocean waves and the basis for analyzing SAR images, *Chin. J. Oceanol. Limnol.*, *28*, Suppl., 1–5.

Zheng, Q., Y. Yuan, V. Klemas, and X.-H. Yan (2001), Theoretical expression for an ocean internal soliton synthetic aperture radar image and determination of the soliton characteristic half width, *J. Geophys. Res.*, *106*, 31,415–31,424, doi:10.1029/2000JC000726.

D. A. Jay, Department of Civil and Environmental Engineering, Portland State University, 1930 SW 4th Avenue, Portland, OR 97201, USA. (djay@cecs.pdx.edu)

H. Lin and J. Pan, Room 615, Esther Lee Building, Institute of Space and Earth Information Science, Chinese University of Hong Kong, Shatin, Hong Kong. (huilin@cuhk.edu.hk; panj@cuhk.edu.hk)